# Proton conducting, composite sulfonated polymer membrane for medium temperature and low relative humidity fuel cells

CrossMark

Dong Won Shin, Na Rae Kang, Kang Hyuck Lee, Doo Hee Cho, Ji Hoon Kim, Won Hyo Lee, Young Moo Lee*

*Department of Energy Engineering, Hanyang University, Seoul 133-791, Republic of Korea*

## HIGHLIGHTS

- Composite membranes show enhanced mechanical property.
- Inorganic filler introduces well-defined hydrophilic ionic clusters into composite membranes.
- Composite membranes outperform pristine membrane at 120 °C and 35% RH.

## ARTICLE INFO

## ABSTRACT

Inorganic—organic composite membranes are fabricated using zirconium acetylacetonate nanoparticles and biphenol-based sulfonated poly(arylene ether sulfone) as an inorganic, proton conducting nano-material and a polymer matrix, respectively. An amphiphilic surfactant (Pluronic®) induces distribution of the inorganic nanoparticles over the entire polymer membrane. The composite membranes are thermally stable up to 200 °C. Zirconium acetylacetonate improves inter-chain interactions and the robustness of polymer membranes resulting in excellent membrane mechanical properties. In addition, composite membranes show outstanding proton conductivity compared to that of the pristine membrane at medium temperatures (80–120 °C) and low relative humidity (<50%) conditions. This improvement is due to the presence of acetylacetonate anions, which bind water molecules and act as an additional proton conducting site and/or medium. Therefore, the composite membranes significantly outperform the pristine membrane in fuel cell performance tests at medium temperatures and low relative humidity.

© 2014 Elsevier B.V. All rights reserved.

## 1. Introduction

Recent research in proton exchange membrane fuel cells (PEMFCs) has been directed at medium temperatures (80–120 °C) and low relative humidity (RH, <50%) due to the higher energy conversion efficiencies, low levels of carbon monoxide poisoning, easier water management, and comparatively simple operating systems found under these conditions [1–3]. Several efforts in the development of aromatic random copolymers based on sulfonated poly(arylene ether)s (SPAEs) [4–9], sulfonated poly(arylene sulfide)s (SPASs) [10–13], sulfonated polyimides (SPIs) [14–18], and polybenzimidazoles (PBIs) [19–21] have sought to achieve the desired properties for PEMFCs. These sulfonated aromatic polymers

are thermally stable up to 200 °C. In addition, they have excellent mechanical properties and high proton conductivity in their fully hydrated states, however, these polymeric materials have low proton conductivity and poor thermal and mechanical properties. These disadvantages must be overcome to in order to use these materials in medium-temperature, low RH PEMFCs [1].

For PEMFCs operating at a medium temperature and low RH, the Grotthuss mechanism is dominant over the vehicle mechanism for proton conduction due to a lower level of water molecules, which play a key role as a proton carrier [1]. In particular, water readily evaporates above 100 °C resulting in low proton conductivity [22]. Various modification methods such as the use of inorganic composites [23–26], ionic liquid composites [27–29], and blends with basic polymers [30–32] have been attempted to overcome these drawbacks. These tuned membranes have relatively high proton conductivity and PEMFC performance compared to pristine membranes at medium temperatures and low RH because inorganic

* Corresponding author. Tel.: +82 2 2220 0525; fax: +82 2 2291 5982.
  *E-mail addresses:* ymlee@hanyang.ac.kr, jms@hanyang.ac.kr (Y.M. Lee).

materials, ionic liquids, and polyacids are able to act as proton conductors and transport media without water molecules [33]. In addition, these composite materials can bind and retain water molecules even under medium temperature and low RH conditions. Water retention is a critical factor affecting fuel cell performance at medium temperatures and low RH, however, some technical challenges remain such as toxicity and leakage of filler materials. These need to be resolved and improved in order to obtain better electrochemical performance.

Among various modification methods, many researchers have focused on the incorporation of inorganic fillers [34]. The inorganic material improves water retention and mechanical properties through inorganic–organic interfacial interactions. Furthermore, inorganic materials with additional proton acceptor or donor sites enhance proton conductivity, however, inorganic materials are not compatible with organic polymers. In addition, high concentrations of inorganic fillers often lead to the formation of agglomerates resulting in low proton conductivity by blocking transport pathways and to poor mechanical strength due to incompatibilities along the organic polymer and inorganic material interface. For these reasons, it is very important to ensure a fine dispersion of inorganic materials in a polymer matrix for enhanced fuel cell performance.

In the present study, a biphenol-based sulfonated poly(arylene ether sulfone) (BPSH) random copolymer with zirconium acetylacetonate (Zr(Acac)) was introduced as an effective proton exchange membrane to investigate the effect of the inorganic material (zirconium acetylacetonate) on electrochemical performance at medium temperatures and low RH.

## 2. Experimental

### 2.1. Materials

4,4′-dichlorodiphenyl sulfone, 4,4′-biphenol, and potassium carbonate were obtained from Alfa Aesar (Ward Hill, MA). Poly(ethylene glycol)-b-poly(propylene glycol)-b-poly(ethylene glycol) (Pluronic® L-64), zirconium acetylacetonate, and N,N-dimethylacetamide (DMAc) were purchased from Sigma–Aldrich (St. Louis, MO). Other solvents including toluene and 2-propanol were supplied from Daejung Chemical (Seoul, Korea).

### 2.2. Membrane preparation

A biphenol-based sulfonated poly(arylene ether sulfone) (BPSH) random copolymer was synthesized and a pristine membrane was prepared using methods reported elsewhere [7]. The degree of sulfonation of BPSH was controlled to 40 mol.% by changing the feed ratio of sulfonated monomer. Zirconium acetylacetonate inorganic filler and Pluronic® L-64 surfactant were added into a 10 wt.% BPSH polymer solution. The mixture was stirred for 3 h and sonicated for another 3 h to disperse the inorganic materials homogeneously. Pristine BPSH and zirconium acetylacetonate composite membranes were fabricated by casting polymer solution onto a glass plate. All membranes were acidified using a 1 M sulfuric acid solution at 80 °C for 2 h and washed with boiling water for another 2 h.

### 2.3. Thermal and mechanical stabilities

Thermo-gravimetric analysis (TGA) was performed using a TGA Q500 (TA Instrument, DE, USA) to estimate the thermal stability of the pristine and composite membranes from 80 to 990 °C with a ramp rate of 10 °C min⁻¹ under a nitrogen atmosphere. All membranes were dried at 120 °C under vacuum for 24 h before measurement to remove residual water.

Tensile stress and elongation at the break point of the membranes were measured using a universal test machine (UTM, AGS-J 500N, Shimadzu, Kyoto, Japan) at 25 °C according to ASTM D882 in order to investigate the mechanical stability.

### 2.4. Macro and microstructure analysis

The particle size of zirconium acetylacetonate dispersed in DMAc was measured using a Zetasizer Nano ZS (Malvern Instruments, UK) with a 633-nm He-Ne laser. The glass cell was flushed with solution several times to avoid air bubbles before slowly adding the solution into the cell. The samples were equilibrated at 25 °C for 10 min prior to measurements.

The distribution of zirconium particles was examined using a scanning electron microscope (SEM) equipped with an energy dispersive X-ray detector (EDX). The membranes were fractured in liquid nitrogen to observe cross-sectional images.

To prepare samples for transmission electron microscope (TEM) observation, the membranes were stained with lead ions (Pb²⁺) by immersion in a lead acetate aqueous solution, rinsed with deionized water several times, and then dried under vacuum. The stained membranes were embedded in epoxy resin, microtomed using an RMC MTX Ultra microtome (RMC Products, Tucson, AZ, USA), and placed on copper grids. The TEM images were obtained using a LIBRA® 120 (Carl Zeiss, Oberkochen, Germany) at an accelerating voltage of 120 kV.

In-situ small angle X-ray scattering (SAXS) was performed at Pohang Accelerator Laboratory (PAL) using a Pohang Light Source (PLS-II, Beamline 4C). The wavelength of the X-rays was 0.0675 nm and the sample-to-detector distance was 1059 mm. A silver behenate standard was used to calibrate the sample-to-detector distance. Scattering images were obtained using a Mar CCD detector with a 60 s exposure time. Scattering data has been corrected for sample transmission and background scattering. The two-dimensional scattering data were analyzed using an in-house software package provided by PAL to obtain radically integrated SAXS intensities versus the scattering vector $q$, where $q = (4\pi/\lambda)\sin(\theta)$, $\theta$ is one-half of the scattering angle and $\lambda$ is the wavelength of the X-ray.

### 2.5. Measurements

Ion exchange capacity values based on weight ($IEC_w$) were measured using a titration method. The protonated membranes were immersed in a 1 N NaCl solution to substitute the proton (H⁺) of the sulfonic acid groups with sodium (Na⁺). The substituted solution was titrated with a 0.01 N NaOH solution using phenolphthalein as an indicator. The $IEC_w$ value was calculated from Eq. (1);

$$IEC_w = \frac{0.01 \times V_{NaOH}}{W_{dry}} \tag{1}$$

where, $W_{dry}$ is the weight of membrane at dry state and $V_{NaOH}$ is volume of NaOH solution which was added to titrate NaCl solution.

Water uptake (WU) was calculated from the mass difference between the dry ($W_{dry}$) and wet ($W_{wet}$) samples and the swelling ratio (SR) was obtained from the dimensional change between the dry ($V_{dry}$) and hydrated ($V_{wet}$) states, as presented in Eqs. (2) and (3), respectively.

$$WU = \frac{W_{wet} - W_{dry}}{W_{dry}} \times 100 \tag{2}$$

$$SR = \frac{V_{wet} - V_{dry}}{V_{dry}} \times 100 \tag{3}$$

Before the measurements, all samples were dried at 120 °C under vacuum to remove water and then immersed in deionized water at 80 °C to measure the weight and the volume of the dry and wet samples, respectively. The dimensions of the membranes were measured using an optical video microscope (SOMETECH, SV-35, Seoul, Korea). A digimatic indicator (Mitutoyo, ID-C112X/1012X, Tokyo, Japan) was used for thickness measurements.

The weight of the dried membranes ($W_{dry}$) was measured after drying under vacuum to determine the water retention at 120 °C and 35% RH. Membrane samples were soaked in water at 100 °C for 24 h in order to fully hydrate the membranes. Furthermore, the hydrated samples were kept in a temperature and humidity controllable chamber at 120 °C and 35% RH for 24 h to measure the weight of partially hydrated membranes ($W_{wet,2h}$). The water retention (WR) was obtained from Eq. (4) [35].

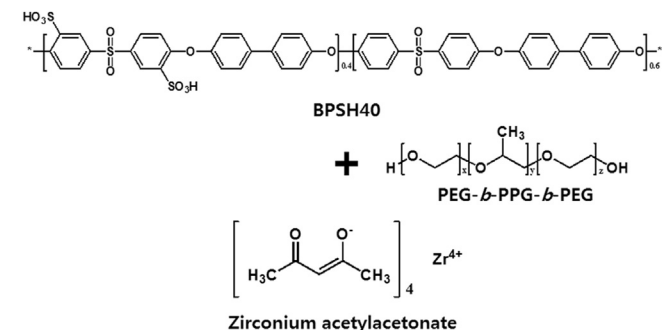$$WR = \frac{\left(W_{wet,2h} - W_{dry}\right)}{W_{dry}} \times 100 \tag{4}$$

The stability to leaching out (LO) of the zirconium acetylacetonate inorganic material was obtained by measuring the difference between the weight of the sodium salt form ($W_{Na}$) and the protonated form ($W_H$). The weight change was calculated using Eq. (5).

$$LO = \frac{(W_{Na} - W_H)}{W_{Na}} \times 100 \tag{5}$$

### 2.6. Electrochemical performance

The proton conductivity of the membranes was measured under various temperature and humidity conditions using a two-probe type homemade cell connected to a PEMFC single-cell test station (CNL, Seoul, Korea). The humidity was controlled by changing the temperature of the humidifier and the conductivity cell under nitrogen flow with 0.15 MPa backpressure. The proton conductivity was calculated by measuring the resistance between the working and counter electrodes. The resistance of the membranes was obtained between 100 mHz and 100 kHz using an alternating current (AC) impedance/gain-phase analyzer (Solartron 1260, Farnborough, Hampshire, UK) and an electrochemical interface (Solartron 1287).

The membrane electrode assembly (MEA) was prepared by attaching catalyst-loaded gas diffusion layers to both sides of the membrane. The electrocatalyst used in the anode and cathode was 20 wt.% Pt/C (Alfa Aesar, Ward Hill, MA, USA) whereas binder was 20 wt.% Nafion® ionomer solutions (Sigma Aldrich, St. Louis, MO, USA). The catalyst slurry was coated on the gas diffusion layer by screen printing. The PEMFC single cell test was conducted under various temperature and humidity conditions (80 °C, 100% RH; 80 °C, 50% RH; and 120 °C, 35% RH) with 0.15 MPa backpressure

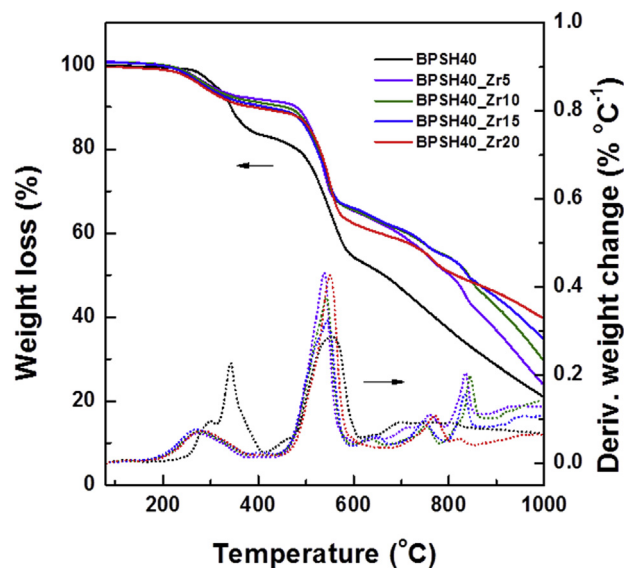**Scheme 1.** Schematic of zirconium acetylacetonate composite BPSH membrane.

**Fig. 1.** TGA thermograms of pristine and inorganic composite BPSH membranes.

using a PEMFC single-cell test station. Hydrogen and air were purged as a fuel and oxidant, respectively.

## 3. Results and discussion

### 3.1. Membrane preparation

The pristine (BPSH40) and composite membranes (BPSH40_ZrXX, where XX is the wt.% of zirconium acetylacetonate with respect to the polymer) with 40 mol.% sulfonation were prepared with similar thicknesses (50–60 μm) to negate any thickness effects on the membrane properties. The zirconium acetylacetonate was composed of one zirconium cation and four acetylacetonate anions, as shown in Scheme 1. These acetylacetonate anions can act as proton conductors by forming hydrogen bonds with the protons.

### 3.2. Thermal and mechanical stabilities

Fig. 1 shows the thermograms of pristine and composite membranes obtained by thermo-gravimetric analysis (TGA). Composite membranes exhibited different thermal decomposition behaviors according to their zirconium acetylacetonate content. Thermal degradation of pristine BPSH40 started from 275 °C, which is associated with thermal decomposition of the sulfonic acid groups [36]. In the case of composite membranes, weight loss started from 190 °C because of thermal evaporation of acetylacetonate groups (boiling point ≈ 187.6 °C at 0.1 MPa) that strongly interacted with sulfonic acid groups. The weight loss of composite membranes was almost the same up to 600 °C resulting from the carbonization and degradation of organic portion of composite membranes. However,

**Table 1**
Mechanical properties of pristine and inorganic composite BPSH membranes.

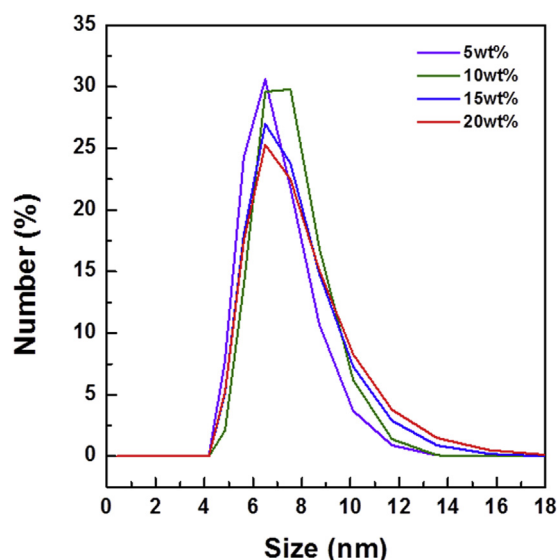|  | Tensile strength [MPa] | Elongation at break [%] | Modulus [MPa] |
|---|---|---|---|
| BPSH40 | 25 | 64 | 680 |
| BPSH40_Zr5 | 33 | 120 | 788 |
| BPSH40_Zr10 | 35 | 105 | 821 |
| BPSH40_Zr15 | 37 | 52 | 895 |
| BPSH40_Zr20 | 38 | 14 | 1017 |

**Fig. 2.** Particle size and distribution of zirconium acetylacetonate.

the residual weight of zirconium after complete pyrolysis of polymer at 990 °C was around 5, 10, 15, and 20 wt.% for BPSH40_Zr5, BPSH40_Zr10, BPSH40_Zr15, and BPSH40_Zr20, respectively. Note that BPSH40 showed a residual weight of 20 wt.%. This result precisely confirms the zirconium contents of composite membranes. The zirconium acetylacetonate is thermally stable up to 190 °C and is a candidate for medium temperature fuel cell application.

Tensile strength and elongation were measured to study the mechanical stability of membrane samples; these results are shown in Table 1. The elongation at break was much higher for the BPSH40_Zr5 membrane (120%) compared to the pristine

membrane (64%), however, elongation gradually declined as more zirconium acetylacetonate was added. An optimized amount of zirconium acetylacetonate may enhance the flexibility of the composite membrane, whereas excess inorganic materials inside the BPSH40 membrane reduce the flexibility due to aggregation of the ionic compound. In the case of composite membranes, zirconium acetylacetonate improved the tensile strength (composite = 33–38 MPa and pristine = 25 MPa). Furthermore, inorganic composite membranes showed a much higher modulus (788–1017 MPa) compared to the pristine membrane (680 MPa) because the inorganic materials improved the robustness of the polymer membranes. As a result, BPSH40_Zr20 membrane has the best mechanical properties among pristine and other composite membranes.

### 3.3. Membrane morphology

The particle size of zirconium acetylacetonate was about 6.5 nm and was independent of the concentration, as shown in Fig. 2. The uniform particle size and narrow size distribution correspond well with the morphology of the composite membranes. The morphology of the BPSH40_Zr20 composite membrane was observed at the macro scale using SEM-EDX, as shown in Fig. 3. The BPSH40_Zr20 membrane showed homogeneity in both SEM and EDX images, indicating that the zirconium acetylacetonate inorganic materials were uniformly distributed throughout the polymer matrix. We attribute the successful dispersion of the zirconium acetylacetonate inorganic nanoparticles throughout the polymeric matrix to the presence of the amphiphilic Pluronic® surfactant.

Fig. 4 shows the micro scale morphology of pristine and composite membranes, analyzed by TEM. The pristine membrane (BPSH40) exhibited a homogeneous distribution of hydrophilic–hydrophobic phases in the TEM image since BPSH40 was randomly composed of hydrophilic and hydrophobic repeating units,
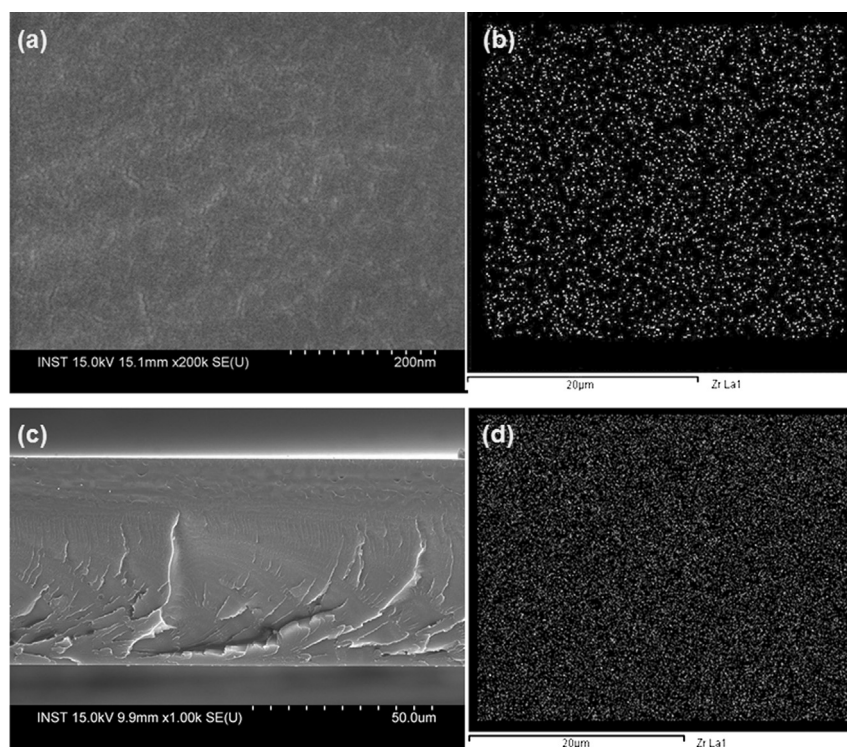


**Fig. 3.** Surface ((a) and (b)) and cross-section ((c) and (d)) morphology images of BPSH40-Zr20 membrane. Zirconium ion (white dots) mapping ((b) and (d)) confirms the homogeneous dispersion of nanoparticles in the polymer matrix.
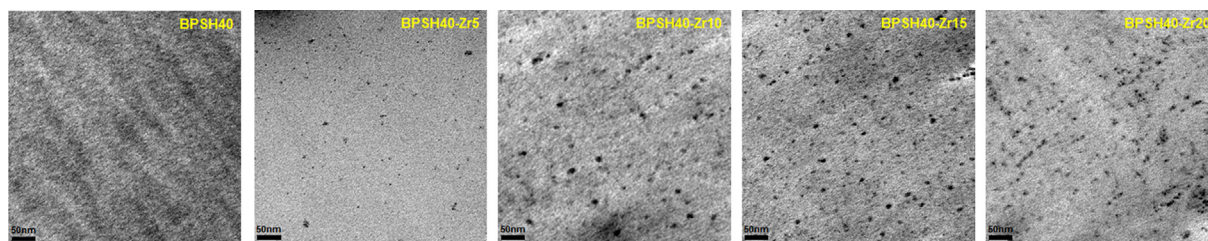
**Fig. 4.** TEM images of pristine and inorganic composite BPSH membranes.

however, the composite membranes had small (5–10 nm) hydrophilic ionic clusters throughout the polymer matrix (these appear as dark regions because they were stained with lead ions). This is possibly due to zirconium acetylacetonate aggregating around the sulfonic acid groups which results in a cluster formation [37]. Consequently, the hydrophilic clusters increased in number as more zirconium acetylacetonate was added into the membrane, as presented in Fig. 5.

The SAXS profiles of the pristine and composite membranes are shown in Fig. 6. The pristine membrane showed a broad scattering profile, while the composite membranes exhibited noticeable scattering maxima ($q_{max}$) in the range of 0.79–0.89 Å$^{-1}$. The interdomain distance ($d$) was obtained from Bragg's law ($d = 2\pi/q_{max}$). Both pristine and composite membranes have inter-domain distances in the range of 7–8 nm, however, the pristine membrane was almost homogeneous and exhibited a featureless scattering pattern. In addition, the intensity of the scattering maxima increased as the content of zirconium acetylacetonate increased from 5 wt.% to 20 wt.%. These scattering patterns correspond well with TEM images and the results from the particle size analysis. Although composite membranes have ionic clusters of similar sizes, the concentration of ionic clusters increased relative to the amount of inorganic material.

### 3.4. Measurements

Table 2 shows the weight-based ion exchange capacity (IEC$_w$) value, water uptake, swelling ratio, water retention, and stability to leaching out of pristine and zirconium acetylacetonate composite membranes. These values can be used to estimate membrane properties as a proton exchange membrane. Although composite membranes contain additional proton conducting sites (acetylacetonate anions), the IEC$_w$ values of the composite membranes were lower than that of the pristine membrane. This is due to the relatively high atomic weight of zirconium (91.22 amu). In addition,
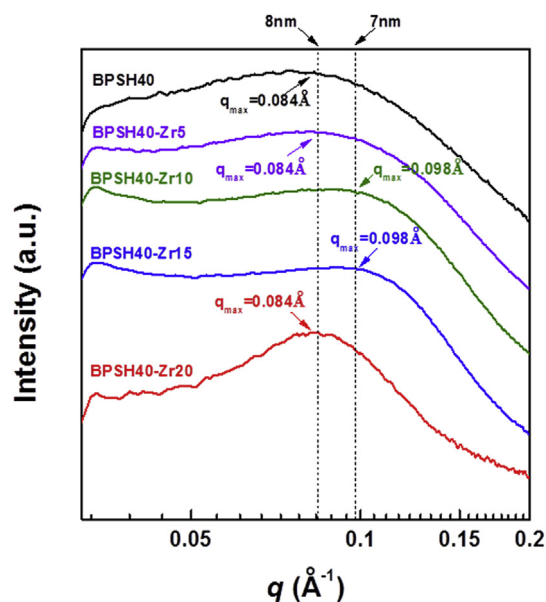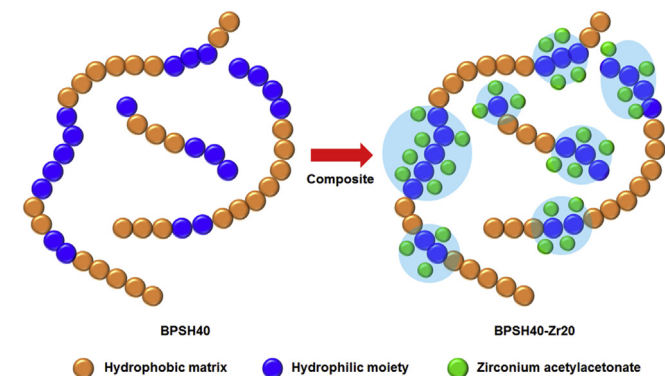


**Fig. 5.** Schematic drawing of morphology images according to inorganic filler content. Zirconium acetylacetonate aggregates into the hydrophilic portions of BHSH40 forming hydrophilic ionic clusters 5–10 nm in size.
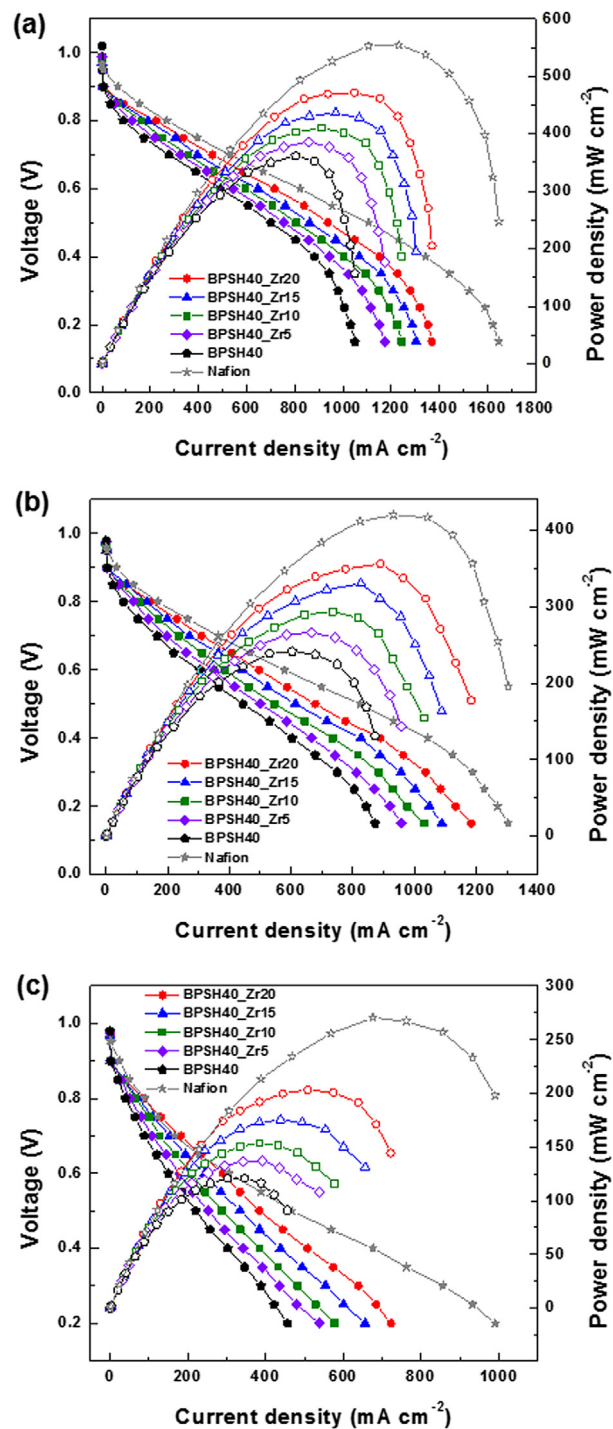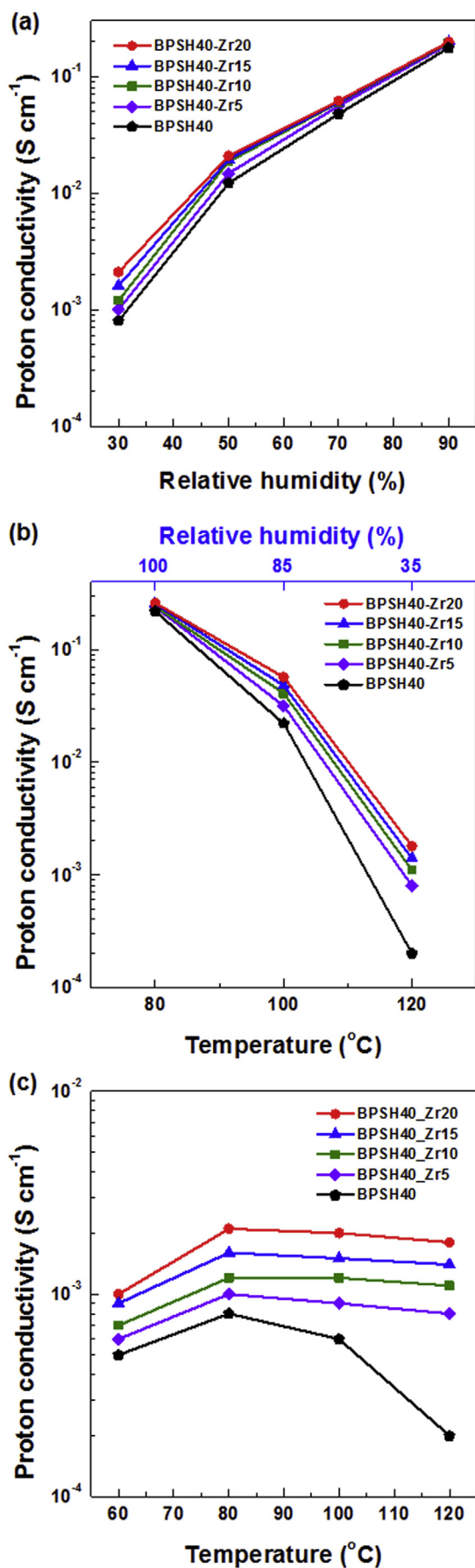


**Fig. 6.** Synchrotron SAXS profiles of the pristine and composite membranes. The interdomain distance for BPSH40_Zr20 samples is 7–8 nm. Pristine and lower nanoparticle concentration membranes did not show any distinct scattering patterns.

the IEC$_w$ slightly decreased with increasing inorganic content. Conversely, composite membranes showed higher water uptake and swelling ratios than the pristine membrane. Furthermore, composite membranes retained higher amounts of water molecules than the pristine membrane at 120 °C and 35% RH because the composite materials are able to retain water molecules above 100 °C. In addition, hydrophilic ionic domains of composite membranes in the 7–8 nm range improved water retention property with capillary phenomena [35]. The stability to leaching out of the inorganic fillers was estimated by measuring the weight change after acidification. Both pristine and composite membranes lost 3.5–4.0 wt.% after acidification. The weight loss may be attributed to the extraction of residual solvent and the conversion of the counter ions of $-SO_3^-$ from Na$^+$ (22.99 amu) to H$^+$ (1.01 amu). Therefore, the composite membranes have excellent stability to leaching out of the zirconium acetylacetonate.

**Table 2**
IEC, water uptake, swelling ratio, water retention, and stability to leaching out (LO) of pristine and inorganic composite membranes.

| | IEC$_w$ [meq g$^{-1}$] | Water uptake [wt.%] | Swelling ratio [vol.%] | Water retention [wt.%] | LO [wt.%] |
|---|---|---|---|---|---|
| BPSH40 | 1.64 | 33 | 38 | 1.2 | 3.5 |
| BPSH40_Zr5 | 1.24 | 37 | 41 | 1.8 | 3.8 |
| BPSH40_Zr10 | 1.20 | 41 | 46 | 2.1 | 3.8 |
| BPSH40_Zr15 | 1.16 | 46 | 50 | 2.3 | 4.0 |
| BPSH40_Zr20 | 1.10 | 52 | 56 | 2.9 | 3.6 |

**Fig. 8.** PEMFC single-cell performance of Nafion® 212, pristine and inorganic composite BPSH membranes at (a) 80 °C, 100% RH, (b) 80 °C, 50% RH, and (c) 120 °C, 35% RH.

### 3.5. Electrochemical performance

The proton conductivity was measured at various temperatures and RH conditions to verify the effect of our proton conducting inorganic materials on proton transport, as shown in Fig. 7. The

**Fig. 7.** Proton conductivity of pristine and inorganic composite membranes at (a) 80 °C as a function of relative humidity, (b) medium temperatures (80–120 °C), and (c) 30% RH as a function of temperature.

proton conductivity of the pristine and composite membranes was quite similar at 80 °C and high RH (>90%), however, when the RH was lowered to 30% (at 80 °C), the composite membranes displayed higher proton conductivity compared to the pristine membrane. Furthermore, composite membranes maintained much of their proton conductivity (relative to their fully hydrated state) above 100 °C, which is the evaporation temperature of water molecules. Conversely, the proton conductivity of the pristine membrane dropped significantly when the temperature was increased to 120 °C and the RH was lowered to 35%. Similarly, proton conductivity of composite membranes depended to a less extent on temperature compared with that of pristine membrane at 30% RH condition in the 60–120 °C range due to excellent water retention property of composite membranes.

Proton exchange membrane fuel cell performance was evaluated at three different temperatures and three different RH conditions in order to investigate the effect of our proton conducting inorganic materials on fuel cell performance, as shown in Fig. 8. Composite membranes showed slightly higher maximum power densities (386–471 mW cm$^{-2}$) compared to the pristine membrane (362 mW cm$^{-2}$) under the fully hydrated condition at 80 °C. Well-defined hydrophilic domains may facilitate through-plane proton transport as well as in-plane direction resulting in an increase in single cell performance despite of similar proton conductivity at hydrated state. This gap in performance widened as the temperature was raised and the relative humidity was reduced. At 80 °C and 50% RH, the maximum power densities of the composite membranes (266–356 mW cm$^{-2}$) were much higher than that of the pristine membrane (241 mW cm$^{-2}$). In addition, the maximum power densities of the pristine membrane (121 mW cm$^{-2}$) decreased significantly as the temperature was increased to 120 °C and the relative humidity was decreased to 35%; the composite membranes maintained much of their performance (137–203 mW cm$^{-2}$) under these conditions. This behavior corresponds well with the proton conductivity results. Although, single cell performances of the BPSH40_Zr20 membrane were relatively lower than those of Nafion® 212 under various temperature and humidity conditions due to low performance of mother polymer material (BPSH40), BPSH40_Zr20 membrane exhibited the highest single cell performance among pristine and other composite membranes. It can be concluded from these results that proton conducting inorganic materials in a polymeric membrane bind and retain water molecules within the material. Thus, the inorganic material added to the PEM improved the proton conductivity and led to higher fuel cell performance, even at medium temperatures and low RH.

## 4. Conclusions

Zirconium acetylacetonate composite BPSH membranes show outstanding mechanical properties compared to the pristine BPSH membrane. Although zirconium acetylacetonate inorganic fillers are uniformly dispersed throughout the polymeric matrix, both pristine and composite membranes show hydrophilic ionic clusters on the order of 7–8 nm. The concentration of hydrophilic ionic clusters increases with the content of the inorganic composite material. These hydrophilic ionic clusters are capable of retaining water molecules at both fully and partially hydrated states. For these reasons, composite membranes show higher proton conductivity than pristine membranes, particularly at low RH. Similarly, the PEMFC single cell performance of composite membranes is highly improved at medium temperatures and low RH compared to the pristine membrane. Consequently, BPSH40_Zr20 membrane represents the best properties such as water retention, proton conductivity, and single cell performance. Thus, zirconium

acetylacetonate has great potential to be utilized as a proton conducting, inorganic material in composite membranes for medium temperature and low RH fuel cell applications.

## References

[1] C.H. Park, C.H. Lee, M.D. Guiver, Y.M. Lee, Prog. Polym. Sci. 36 (2011) 1443.
[2] A. Chandan, M. Hattenberger, A. El-Kharouf, S.F. Du, A. Dhir, V. Self, B.G. Pollet, A. Ingram, W. Bujalski, J. Power Sources 231 (2013) 264.
[3] J.L. Zhang, Z. Xie, J.J. Zhang, Y.H. Tanga, C.J. Song, T. Navessin, Z.Q. Shi, D.T. Song, H.J. Wang, D.P. Wilkinson, Z.S. Liu, S. Holdcroft, J. Power Sources 160 (2006) 872.
[4] B. Bae, K. Miyatake, M. Watanabe, J. Membr. Sci. 310 (2008) 110.
[5] D.S. Kim, K.H. Shin, H.B. Park, Y.S. Chung, S.Y. Nam, Y.M. Lee, J. Membr. Sci. 278 (2006) 428.
[6] Y.S. Kim, M.A. Hickner, L.M. Dong, B.S. Pivovar, J.E. McGrath, J. Membr. Sci. 243 (2004) 317.
[7] F. Wang, M. Hickner, Y.S. Kim, T.A. Zawodzinski, J.E. McGrath, J. Membr. Sci. 197 (2002) 231.
[8] Y.S. Kim, B. Einsla, M. Sankir, W. Harrison, B.S. Pivovar, Polymer 47 (2006) 4026.
[9] N. Li, C. Wang, S.Y. Lee, C.H. Park, Y.M. Lee, M.D. Guiver, Angew. Chem. Int. Ed. 50 (2011) 9158.
[10] S.Y. Lee, N.R. Kang, D.W. Shin, C.H. Lee, K.S. Lee, M.D. Guiver, N. Li, Y.M. Lee, Energy Environ. Sci. 5 (2012) 9795.
[11] D.W. Shin, S.Y. Lee, N.R. Kang, K.H. Lee, M.D. Guiver, Y.M. Lee, Macromolecules 46 (2013) 3452.
[12] M. Schuster, C.C. de Araujo, V. Atanasov, H.T. Andersen, K.D. Kreuer, J. Maier, Macromolecules 42 (2009) 3129.
[13] M. Schuster, K.D. Kreuer, H.T. Andersen, J. Maier, Macromolecules 40 (2007) 598.
[14] J.H. Fang, F.X. Zhai, X.X. Guo, H.J. Xu, K. Okamoto, J. Mater. Chem. 17 (2007) 1102.
[15] B.R. Einsla, Y.S. Kim, M.A. Hickner, Y.T. Hong, M.L. Hill, B.S. Pivovar, J.E. McGrath, J. Membr. Sci. 255 (2005) 141.
[16] C. Perrot, L. Gonon, C. Marestin, G. Gebel, J. Membr. Sci. 379 (2011) 207.
[17] G. Meyer, G. Gebel, L. Gonon, P. Capron, D. Marscaq, C. Marestin, R. Mercier, J. Power Sources 157 (2006) 293.
[18] K. Miyatake, H. Furuya, M. Tanaka, M. Watanabe, J. Power Sources 204 (2012) 74.
[19] N. Xu, X.X. Guo, J.H. Fang, H.J. Xu, J. Yin, J. Polym. Sci. Polym. Chem. 47 (2009) 6992.
[20] L. Xiao, H. Zhang, T. Jana, E. Scanlon, R. Chen, E.W. Choe, L.S. Ramanathan, S. Yu, B.C. Benicewicz, Fuel Cells 5 (2005) 287.
[21] H.J. Kim, S.J. An, J.Y. Kim, J.K. Moon, S.Y. Cho, Y.C. Eun, H.K. Yoon, Y. Park, H.J. Kweon, E.M. Shin, Macromol. Rapid Commun. 25 (2004) 1410.
[22] W. Dai, H.J. Wang, X.Z. Yuan, J.J. Martin, D.J. Yang, J.L. Qiao, J.X. Ma, Int. J. Hydrogen Energ. 34 (2009) 9461.
[23] Y. Choi, Y. Kim, H.K. Kim, J.S. Lee, J. Membr. Sci. 357 (2010) 199.
[24] J.H. Chang, J.H. Park, G.G. Park, C.S. Kim, O.O. Park, J. Power Sources 124 (2003) 18.
[25] Y. Kim, Y. Choi, H.K. Kim, J.S. Lee, J. Power Sources 195 (2010) 4653.
[26] J.H. Piao, S.J. Liao, Z.X. Liang, J. Power Sources 193 (2009) 483.
[27] E. van de Ven, A. Chairuna, G. Merle, S.P. Benito, Z. Borneman, K. Nijmeijer, J. Power Sources 222 (2013) 202.
[28] M. Martinez, Y. Molmeret, L. Cointeaux, C. Iojoiu, J.C. Lepretre, N. El Kissi, P. Judeinstein, J.Y. Sanchez, J. Power Sources 195 (2010) 5829.
[29] T. Yasuda, S. Nakamura, Y. Honda, K. Kinugawa, S.Y. Lee, M. Watanabe, ACS Appl. Mater. Interfaces 4 (2012) 1783.
[30] Y.S. Kim, F. Wang, M. Hickner, T.A. Zawodzinski, J.E. McGrath, J. Membr. Sci. 212 (2003) 263.
[31] J.A. Mader, B.C. Benicewicz, Macromolecules 43 (2010) 6706.
[32] X.B. Chen, P. Chen, Z.W. An, K. Chen, K. Okamoto, J. Power Sources 196 (2011) 1694.
[33] S. Bose, T. Kuila, X.L.N. Thi, N.H. Kim, K.T. Lau, J.H. Lee, Prog. Polym. Sci. 36 (2011) 813.
[34] B.P. Tripathi, V.K. Shahi, Prog. Polym. Sci. 36 (2011) 945.
[35] S.Y. Lee, D.W. Shin, C. Wang, K.H. Lee, M.D. Guiver, Y.M. Lee, Electrochem. Commun. 31 (2013) 120.
[36] S. Tan, D. Belanger, J. Phys. Chem. B 109 (2005) 23480.
[37] T. Kim, Y.W. Choi, C.S. Kim, T.H. Yang, M.N. Kim, J. Mater. Chem. 21 (2011) 7612.